Ultrasonics 91 (2019) 45–51

Contents lists available at ScienceDirect

Ultrasonics

journal homepage: www.elsevier.com/locate/ultras

Examination of the temperature influence on phase matching frequency in tunable acousto-optic filters

S.N. Mantsevich[a,b,*], E.I. Kostyleva[a]

[a] Physics Department, M.V. Lomonosov Moscow State University, GSP-2, Vorobevy Gory, 119991 Moscow, Russia
[b] Space Research Institute (IKI), 84/32 Profsoyuznaya, 117997 Moscow, Russia

ARTICLE INFO

Keywords:
Acousto-optic interaction
Acousto-optic phase matching condition
Temperature
Tellurium dioxide
Acoustic beam attenuation
Phase matching temperature shift

ABSTRACT

The temperature effect on the acousto-optic (AO) phase matching condition was examined both theoretically and experimentally on an example of wide-angle acousto-optic filter fabricated from tellurium dioxide crystal. It was shown that the AO crystal temperature variation changes the acoustic wave velocity that is involved into the AO interaction and shifts the phase matching frequency of AO diffraction. The AO phase matching frequency shift temperature coefficient was introduced, characterizing the magnitude of the frequency shift. The examination of frequency shift magnitude was carried for the optical wavelength band from 440 nm to 1.52 μm. It was shown that the temperature coefficient decreases with increasing the optical wavelength. A method was introduced that makes it possible to calculate the temperature shift coefficients for the real AO devices in a wide range of optical wavelengths. The coefficients obtained with the proposed method are in good agreement with the experimental data. Ultrasound attenuation was also examined in the given AO cell. Attenuation caused by the acoustic power absorption is the main mechanism leading to the appearance of the inhomogeneous temperature distribution inside the AO cell during the operation.

1. Introduction

Optoelectronic devices operating on the basis of acousto-optic (AO) effect are widely used for optical radiation control and its spectrum analysis nowadays [1].

Such advantages of AO devices are a small size, the absence of moving parts, comparatively low power consumption and high reliability make them attractive for the fabrication of compact spectral analysis instruments. Such devices may be used not only in laboratory conditions but also outdoors and even in space [2–8]. One of the peculiarities that arise when using AO instruments outside the laboratory and strongly affecting the parameters of acousto-optical devices is a wide operation temperature range. In space it may exceed 100 K. Due to the difficulties with AO crystal temperature stabilization the problem of AO crystal temperature influence on the AO devices characteristics arises. The solution of this problem is important especially for the AO tunable filters (AOTFs). It will allow avoiding the mistakes during the experimental data analysis associated with the recognition of various substances buy their optical radiation absorption bands. These mistakes are caused by the observed displacement of the examined substances absorption bands due to a change in the temperature of the AO crystal [9].

There are two mechanisms that influence on the AO cell temperature. The first one is the heating or cooling of the AO crystal under the action of ambient temperature [2,10,11]. The second one is the inhomogeneous heating of the AO cell upon the absorption of the acoustic beam power by the material of the AO cell [12–14]. The AO device temperature may be stabilized in the first case, the equalization of temperature gradients during the AO cell operation seems to be much more difficult.

The AO devices are usually fabricated from the crystalline materials that have strong anisotropy of various physical properties. For example, the most popular AO material – tellurium dioxide is known for its extremely high acoustic anisotropy [15,16].

The crystalline media characteristics which are important for AO interaction realization (namely the acoustic wave velocity and the refraction indices) depend on temperature [17–20]. Hence, the characteristics of AO devices depend on temperature also [7,10,12,21]. Theoretical and experimental examination of temperature influence on TeO_2 AOTF operation was carried for the wide range of optical radiation wavelengths. We have also measured the acoustic beam attenuation to examine the inhomogeneous temperature distribution occurring inside the TeO_2 AO cell during the operation.

* Corresponding author at: Physics Department, M.V. Lomonosov Moscow State University, GSP-2, Vorobevy Gory 1, bd. 2, 119991 Moscow, Russia.
E-mail address: snmantsevich@yahoo.com (S.N. Mantsevich).

https://doi.org/10.1016/j.ultras.2018.07.016
Received 14 May 2018; Received in revised form 22 July 2018; Accepted 24 July 2018
Available online 25 July 2018

2. The examination of crystal temperature effect on AO phase matching condition

2.1. Basic relations

The crystal temperature influences mainly the acoustic wave propagation velocity [17–20,22]. This may be explained in the following way. It is known that the acoustic wave velocity in the crystal may be defined by solving the Christoffel equation:

$$|\Gamma_{jk} - \rho V^2 \delta_{jk}| = 0 \quad (1)$$

where ρ – is the density, V – acoustic wave phase velocity, δ_{jk} – Kronecker delta, and Γ_{jk} defined as $\Gamma_{jk} = c_{ijkl} n_i n_l$ – is the second-rank tensor. The elastic modules matrix elements c_{ij} change with temperature in the following way:

$$\frac{dc_{ij}}{dT} = \gamma_{ij} c_{ij} \quad (2)$$

where γ_{ij} – are the elements of thermal coefficients matrix for c_{ij}. Based on the evidences [17–20], one may consider that the temperature dependence $c_{ij}(T)$ is linear. It was shown in papers [10,22] that the best correspondence between the theoretical calculations and experimental results is obtained by using the $c_{ij}(T)$ data presented in [19]. The values of TeO_2 elastic modules c_{ij} and their thermal variation dc_{ij}/dT are presented in Table 1.

In the presented investigation the temperature influence examination was carried for the wide-aperture AOTF fabricated from TeO_2 crystal with 10.5° cut-angle. The AO interaction is realized in $(1\bar{1}0)$ plane, the incident optical radiation has extraordinary polarization. Solving the Eq. (1) it is possible to obtain that the acoustic energy walk-off angle along the chosen direction is as high as 54.6°; the slow shear acoustic wave velocity is 716 m/s for the 10.5° cut-angle.

Using the Eqs. (1) and (2) for the case of slow acoustic wave propagating at 10.5°to the crystallographic [1 1 0] axis the following temperature coefficient showing the variation of ultrasound wave velocity with temperature was obtained: 0.06 m/s·K^{-1}. This value seems to be rather low, but it is enough to influence AO diffraction characteristics significantly. We need to mention here that both acoustic wave velocity and its variation with temperature [22] depend on the chosen direction in TeO_2 crystal.

It is convenient to use wave vector diagram method for the AO interaction description [23]. The following relation takes place for wave vectors of incident $\vec{k}_i$ and diffracted $\vec{k}_d$ optical waves and acoustic wave vector $\vec{K}$ in the case of phase matching condition fulfilled:

$$\vec{k}_d = \vec{k}_i + \vec{K} \quad (3)$$

where $|\vec{k}_i| = 2\pi n_i/\lambda$; $|\vec{k}_d| = 2\pi n_d/\lambda$; $|\vec{K}| = 2\pi f/V$, f – ultrasound frequency, V – ultrasound velocity and λ – optical radiation wavelength.

The wave vector Eq. (3) may be illustrated by the following drawing, presented in Fig. 1.

The n_o and n_e are the segments of refractive indices surfaces cross sections by the $(1\bar{1}0)$ plane, $\alpha = 10.5Â°$, $\theta_i = 25Â°$.

Using the presented vector diagram it is possible to obtain the equation that defines the AO interaction phase matching frequency. It will be the following in the case of extraordinary polarization of incident optical beam:

$$f = \frac{V(T)}{\lambda}\{\sqrt{n_o^2 - n_i^2 \cos\Theta_B} - n_i \sin\Theta_B\}, \quad (4)$$

where n_i is the refraction coefficient for the incident optical beam, T is the crystal temperature and Θ_B is the Bragg angle.

In fact, the values of the refraction indices also depend on the temperature, but there is no reliable data allowing taking into account their variation with temperature for paratellurite in IR region. Also the effect of their variation on the AO synchronism frequency is much less than the ultrasound wave velocity change. So we will consider n_i and n_o to be constant and depending only on the optical wavelength.

The TeO_2 refraction indices were calculated with the following equation [24]:

$$n^2 = 1 + \frac{C_0\lambda^2}{\lambda^2 - C_2^2} + \frac{C_1\lambda^2}{\lambda^2 - C_3^2} \quad (5)$$

where λ is the optical radiation wavelength in μm, and C_i coefficients values are presented in Table 2 [24].

The n_i value was calculated by taking into account the TeO_2 optical activity [25]:

$$n_i = \frac{(n_o + dn)n_e}{\sqrt{n_e^2(\sin\varphi)^2 + (n_o + dn)^2(\cos\varphi)^2}} \quad (6)$$

where dn is the variation caused by optical activity and $\varphi = 90 - \theta_i$ is the angle measured from [1 1 0] axis in $(1\bar{1}0)$ plane defining the incident optical wave propagation direction in crystal.

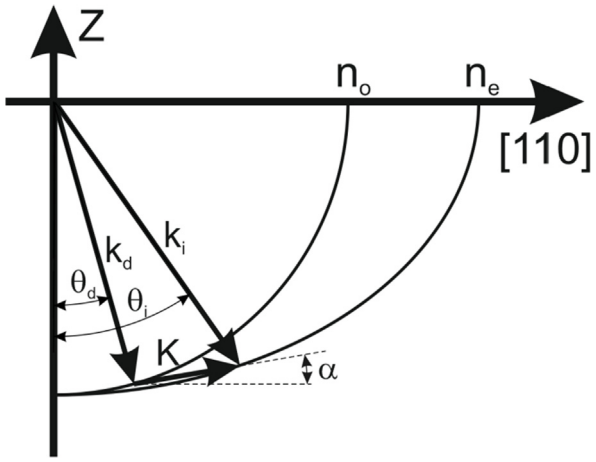

Fig. 1. The wave vector diagram of the AO interaction geometry being examined.

Table 1
The TeO_2 elastic modules and their temperature variation.

c_{ij},10^{10}N/m^2 at 20 °C temperature		$\frac{dc_{ij}}{dT}$, 10^8N/m^2·K^{-1}
c_{11}	5.612	−0.144
c_{12}	5.155	−0.157
c_{13}	2.303	−0.038
c_{33}	10.571	−0.324
c_{44}	2.668	−0.030
c_{66}	6.614	−0.226

2.2. Experimental and computation results

The experimental part of the study was carried with the help of AO cell fabricated from TeO_2 crystal with cut-angle $\alpha = 10.5Â°$, and $\Theta_B = -14.5Â°$. This geometry corresponds to wide-aperture AO interaction geometry [26,27]. The AO interaction length in the chosen AO cell was 0.7 cm. The AOTF passband is about 330 kHz. Various types of lasers were used as the optical radiation sources – gas lasers with 440 nm, 633 nm, 1.15 μm, 1.52 μm (He-Cd and He-Ne lasers

Table 2
The C_i coefficients for evaluation of paratellurite refraction coefficients.

	C_0	C_1	C_2	C_3
n_o	3.71789	0.07544	0.19619	4.61196
n_e	4.33449	0.14739	0.20242	4.93667

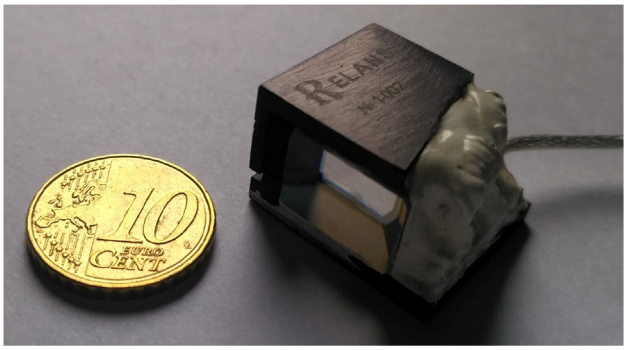

Fig. 2. The photo of the AO cell being examined.

correspondingly) wavelengths and semiconductor lasers with 530 nm and 790 nm wavelengths.

The temperature of AO crystal was controlled both by thermal sensor mounted on its face and infrared imager. The photo of the AO cell being examined is presented in Fig. 2.

Since in this work it was supposed to examine the crystal temperature influence on the AO interaction characteristics, it was necessary to achieve the most homogeneous temperature distribution within the AO cell. To minimize the heating of the crystal due to the ultrasound absorption, the high-frequency generator operated in the amplitude modulation mode by the short rectangular pulses.

The infrared imager was used to control the AO cell temperature homogeneity. The observed AO temperature distributions during the measurements are presented in Fig. 3.

The homogeneous temperature distribution inside the AO cell during the measurements is required to minimize the additional distortions of AOTF transmission function, which appear when temperature gradients inside crystal exist [12,28]. It was found during the experiments that the best way to obtain the homogeneous temperature distribution in the AO crystal is to heat it up to the maximal temperature with 5 degrees margin and to carry the measurements while the crystal cools down slowly due to heat exchange with the environment.

The results of AO phase matching frequency measurements and computations using Eqs. (4)–(6) for various optical wavelengths obtained for the AO cell temperature +25 °C are presented in Table 3 together with temperature coefficients (kHz/K) of AO phase matching frequency shift.

The Fig. 4 shows the comparison of experimental and theoretical dependences of AO phase matching frequency on the optical radiation wavelength (dispersion curves).

So we may conclude that theory and experiment are in good agreement.

Table 3
The theoretically calculated and experimentally measured AO phase matching frequencies and the temperature coefficients of the examined AO cell.

Optical wavelength λ, μm	AO phase matching frequency, MHz		Temperature coefficients of AO phase matching frequency shift, kHz/K	
	Theory	Experiment	Theory	Experiment
0.440	209.80	206.52	17.5	22.6
0.530	159.34	157.67	13.2	16.4
0.633	126.46	126.44	10.5	13.1
0.790	96.82	96.95	8.1	10.4
1.150	64.06	64.34	5.4	6.5
1.390	52.02	52.81	4.3	5.25
1.520	47.28	47.90	3.9	4.6

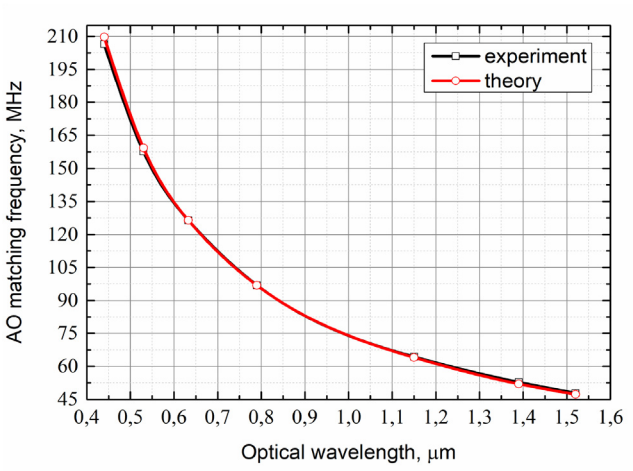

Fig. 4. The comparison of experimental and theoretical dispersion curves of the AOTF being examined.

The AO cell was heated till +65 °C temperature to measure the AO phase matching frequency shift temperature coefficients. The measurements were carried every five degrees. The measurement results were approximated by a linear dependence, and the temperature coefficient was determined from its slope angle.

The comparison of theoretical and experimental AO phase matching frequency shift temperature coefficients presented in Table 3 is shown in Fig. 5.

Curve *1* in Fig. 5 illustrates the experimental measurements AO phase matching frequency shift temperature coefficients. Curve *2* represents the results of the calculations made with Eqs. (1)–(6) and is

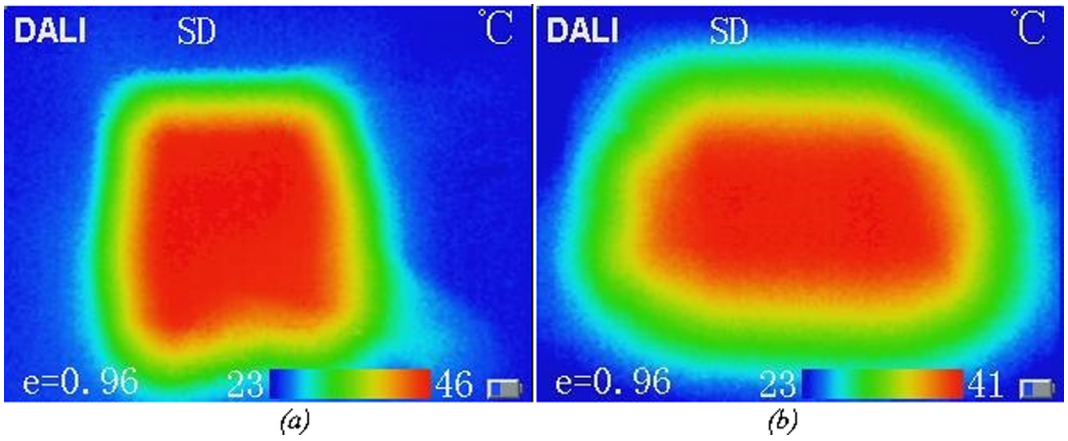

Fig. 3. The images of AO cell temperature distribution during the measurements; a – top view, b – view from the input optical face side.

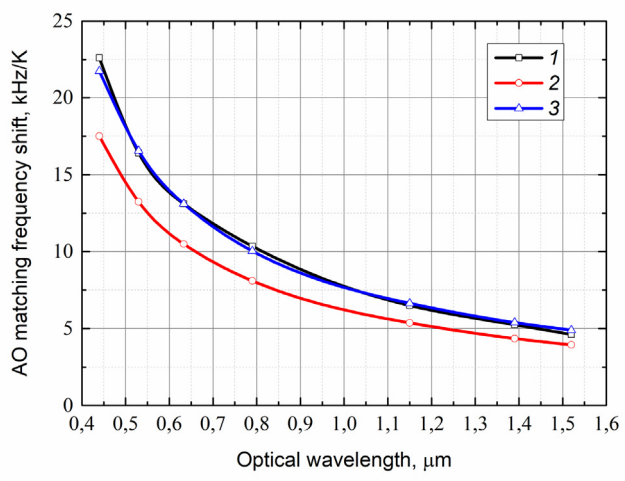

Fig. 5. The comparison of theoretical and experimental AO phase matching frequency shift temperature coefficients; 1 – experiment, 2 – theory, 3 – hybrid method.

based on the data presented in paper [19]. We should notice that, from Eq. (6), and assuming refractive indices to be constant is possible to say that the ratio of theoretical phase matching frequency and temperature coefficient is constant:

$$\frac{f}{df/dT} = \frac{V}{dV/dT} = const \tag{7}$$

though this is not quite so according to the experimental data. The discrepancy between the curves *1* and *2* is also significantly large. That is why there is a need to improve the accuracy of theoretical calculations. We propose a hybrid method (both theoretical and experimental) that includes only one experimental measurement and has a much greater predictive power (curve *3*) then a purely theoretical approach illustrated by curve *2*.

The essence of the hybrid method is the following. The AO phase matching frequency variation with temperature depends only on the change of acoustic wave velocity as follows from Eq. (4). The other multipliers in the right side of the equation doesn't depend on temperature, thereby the Eq. (4) may be rewritten as:

$$\frac{df}{dT} = \frac{dV}{dT}\frac{1}{\lambda} \cdot const \tag{8}$$

The dV/dT derivative we could either take from literature [17–20] or measure in an experiment. In the first case we will obtain curve 2 in Fig. 5. In the second case we could define it by measuring df/dT only for one optical wavelength. It is possible to obtain dV/dT from Eq. (8) if we know df/dT value. This dV/dT value is used further for the calculation of AO phase matching frequency shifts for all other optical wavelengths. As follows from the presented results the hybrid method is in good agreement with experimental results. The use of this method greatly simplifies the AO devices temperature calibration procedures since the measurements should be carried out only at the single optical wavelength. We have used the measurements at 0.633 μm to obtain curve *3*. The AO phase matching frequency shift temperature coefficients calculated using the hybrid method are presented in Table 4.

Table 4
The AO phase matching shift temperature coefficients calculated with the hybrid method for the examined AO cell.

Optical wavelength, μm	0.44	0.53	0.633	0.79	1.15	1.39	1.52
Temperature coefficients of AO phase matching frequency shift, kHz/K (curve *3*)	21.8	16.6	13.1	10.0	6.6	5.4	4.9

The small discrepancies between the results of hybrid calculations and the experiment near the borders of examined optical wavelength band are apparently due to a change of the paratellurite refraction indices with temperature that we can't take into account in the calculations due to the lack of data.

Considering the date presented in Tables 3 and 4 we may conclude that 15 °C temperature variation is enough to shift AOTF transmission function by an amount greater than filter transmission function in the case of 440 nm optical wavelength. At the same time, if we want to obtain the same frequency shift for an 1.52 μm optical wavelength the change in AO crystal temperature of more than 65 degrees is needed. We should also point out that the results presented in Tables 3 and 4 are valid only for the 10.5° cut-angle, but the method proposed may be used for the arbitrary acoustic wave propagation in crystal.

2.3. Examination of ultrasound attenuation

It was mentioned above that the second effect that influences the AO cell temperature is the ultrasound wave power absorption by the material from which it is fabricated. The absorption causes the appearance of the inhomogeneous temperature distribution inside the AO cell. In this case the AO interaction in various parts of the AO crystal occurs at various conditions. The consequence of this effect is asymmetric distortion and additional broadening of the AOTF transmission function [12,28].

Fig. 6 represents the experimentally observed temperature distribution inside the examined AOTF that takes place when it is being connected to the RF generator operating in the continuous mode at the 120 MHz frequency.

It is possible to notice that the maximal temperature gradient is observed near the transducer (in the right part of the AO cell), so the area of maximal heating produced by the acoustic wave power absorption and losses in the electrical matching circuit of the AO cell is located near the transducer [13,14]. The temperature variation along the crystal in the presented case is approximately 7 degrees. Since the maximum temperature inhomogeneity is observed near the AO cell transducer, all measurements presented in the previous part of the paper were carried out for a laser beam passing through the central region of the AOTF, where the temperature gradient is much smaller. This was an additional measure to reduce the influence of possible inhomogeneous temperature distribution that may appear even in the RF generator pulse operation mode.

It is known that in the Bragg regime of AO interaction the intensity of diffracted optical radiation is defined by the following equation:

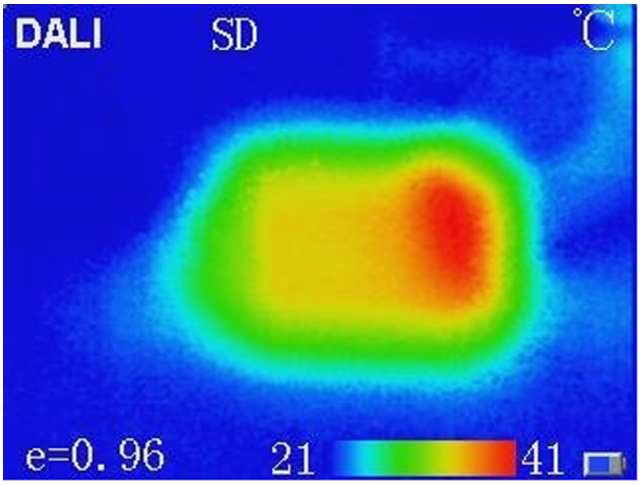

Fig. 6. The image of AO cell temperature distribution in the case of RF generator operation in continuous mode.

$$I_1(l) = I_i\left(\frac{ql}{2}\right)^2 sinc^2\left(\frac{ql}{2\pi}\right) = I_i sin^2\left(\frac{ql}{2}\right) \quad (9)$$

when the phase matching condition is fulfilled.

This equation in the case of low diffraction efficiency approximation may be rewritten in the following form:

$$I_1(l) = \left(\frac{ql}{2}\right)^2 \quad (10)$$

where q is the AO coupling coefficient, defined as:

$$q \sim \sqrt{\frac{MP_a}{lb}} \quad (11)$$

Here M is the acousto-optic figure of merit, P_a – ultrasound power, l – AO interaction length, b – the height of acoustic beam. The ql is called Raman-Nath parameter that equals π in the case of 100% AO diffraction efficiency. It follows from Eqs. (9)–(11) that it is possible to observe the ultrasound beam power variations by measuring the intensity of diffracted optical beam for the incident optical beam passing through the AO cell at various distances from the transducer. Thus it is possible to examine the acoustic wave attenuation in the material of the AO cell.

The results of acoustic power distribution in the AO cell obtained for various frequencies are presented in Fig. 7. The measurements were fulfilled for four largest AO phase matching frequencies, which correspond to optical wavelengths 440, 530, 633 and 790 nm (206.5, 157.7, 126.4 and 96.9 MHz respectively). It is known from literature [29] that the dependence of acoustic power on distance in paratellurite is rather complicated. Unfortunately the AO cell dimensions allowed carrying the measurements only up to a distance 8.5 mm from the transducer. This distance in not enough to obtain the part of the power on distance dependence that should be approximated by exponential dependence as it is known that in isotropic media the attenuation obeys Bouguer's law [29]:

$$I(L) = I_0 e^{-k_f L} \quad (12)$$

where I_0 is the intensity of the signal on the media input, L is the layer thickness of the media through which the wave passes, k_λ is the attenuation coefficient. The thickness L in our case is defined by the distance from the transducer plane to the axis of the laser beam. The correct approximation is possible only for the case of 206.5 MHz acoustic frequency.

The experimental results were approximated by exponentials. The value of k_f coefficient for 206.5 MHz is 0.39 cm^{-1}.

Using the experimental data it is also possible to plot the dependences of the normalized acoustic wave power on the frequency at various distances from the transducer. The results of experimental measurements for the ultrasonic frequencies in the range from 96.9 MHz to 206.5 MHz are presented in Fig. 8.

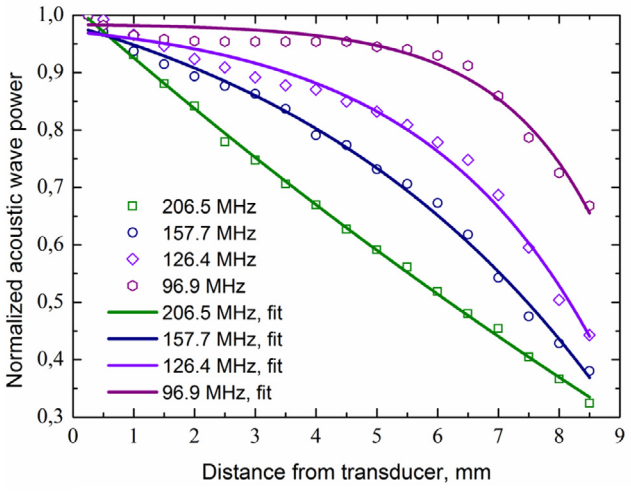

Fig. 7. The dependences of normalized acoustic wave power in the AO cell on distance from transducer for various ultrasound frequencies.

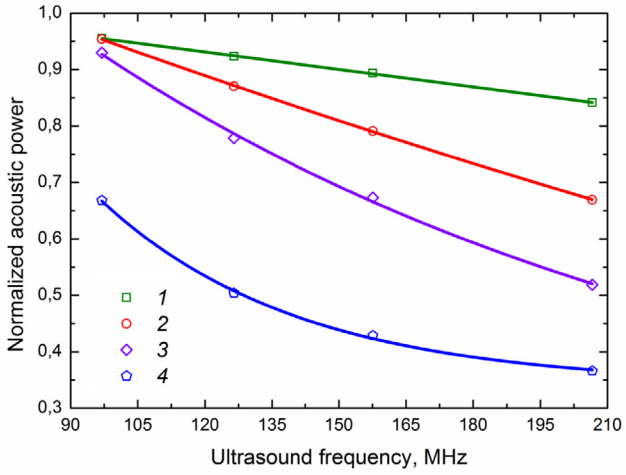

Fig. 8. The dependence of normalized acoustic beam power on ultrasound power at various distances; 1 – L = 2 mm, 2 – L = 4 mm, 3 – L = 6 mm, 4 – L = 8 mm.

The dependence illustrated by curve *1* corresponds to the L = 2 mm, dependence *2* – 2 mm, curves *3* and *4* to 6 and 8 mm respectively.

It is usually considered that the ultrasound wave's attenuation in the medium is proportional to their frequency in the second power, but it can be seen from Fig. 8 that for the small distances from the piezoelectric transducer the dependence is linear. The nonlinearity appears at distances greater than 6 mm in the examined AO cell.

Thus, the absorption of the acoustic wave power by paratellurite is a complex process that does not fit into the framework of usual concepts. The reason for the observed effects in the part of ultrasound absorption is apparently the strong acoustic anisotropy of tellurium dioxide that influences the distribution of acoustic energy inside the beam.

2.4. The examination of acoustic absorption influence on the AOTF transmission function

The absorption of the acoustic power of ultrasonic waves by a paratellurite crystal was examined in the previous section of the paper. It was shown that even at a small distance from the piezoelectric transducer, a significant change in the power of the acoustic wave may occur. This variation affects the AO interaction efficiency. The entire linear aperture of the AO filters is used in acousto-optical devices. Thus, it turns out that in the case of a wide optical beam, light passing through the AO crystal at various distances from the transducer will diffract in an acoustic field with different efficiency. Therefore, it was decided to investigate the change in the shape of the AOTF transmission function from the distance to the transducer plane [29,30]. The results of the transmission function measurements carried out for 440 nm optical wavelength and 0.25 mm, 4 mm, 8.5 mm distances from transducer are presented in Fig. 9.

The experimental data analysis has shown that the diffraction efficiency reduces and the transmission function is broadening with the growth of the distance from the. The results obtained for λ = 440 nm are presented in Table 5.

It turned out that by increasing L from 0.25 mm to 8.5 mm the AO diffraction efficiency is reduced by 70%, and AOTF passband is increased by 15%. The shape of the transmission function transforms slightly also – the side lobes are smoothed out.

Transformations of the AOTF transmission function shape and a decrease in the diffraction efficiency can be explained by the decrease in the AO interaction effective length caused by the ultrasound power

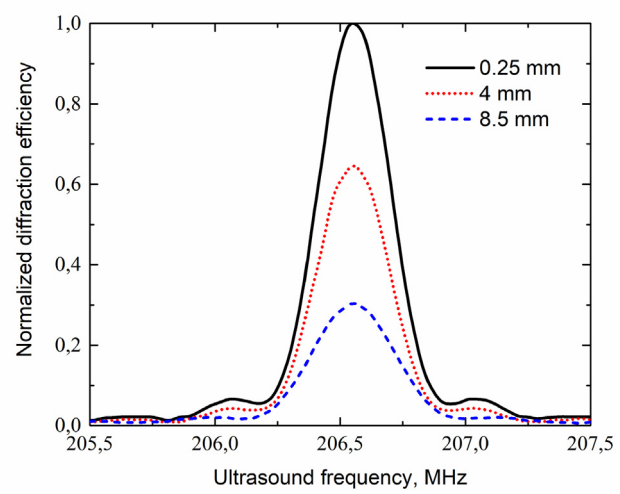

Fig. 9. The AOTF transmission functions measurements at $\lambda = 440$ nm for various distances from transducer.

Table 5
The parameters of the AOTF transmission functions obtained for $\lambda = 440$ nm and various L values.

Distance from optical beam axis to transducer plane, mm	0.25	4	8.5
Transmission function passband, kHz	334	335	386
Normalized diffraction efficiency	1	0.64	0.3

absorption by a tellurium dioxide from which the examined AO cell was fabricated [23,29].

Thus, when performing experimental measurements with the AO filters, it is necessary to take into account the transmission function dependence not only on the temperature, but also on the region in the crystal through which the optical beam passes.

3. Conclusions

AO devices, because of their small dimensions and reliability, are convenient for use not only in laboratory, but also in field conditions, in which the temperature of the AO crystal is difficult to stabilize. For this reason, it is necessary to examine the effect of temperature on the AO filter characteristics.

AO cell fabricated from the paratellurite crystal with a cut-angle angle $\alpha = 10.5$Â°, and $\Theta_B = -14.5$Â° was examined in the presented paper. Both theoretical and experimental examination of the temperature effect on the AO phase matching condition frequency was made for different optical radiation wavelengths.

The AO phase matching frequency shift temperature coefficient was introduced, characterizing the magnitude of the frequency shift in kHz with a change in the crystal temperature by one degree K. It was shown that the temperature coefficient decreases with increasing the optical wavelength. The ratio of the phase matching frequency and the shift magnitude stays constant with the wavelength according to the theoretical evaluations; however, this condition is not fulfilled strictly in the experiment.

A method has been developed that makes it possible to calculate the temperature shift coefficients for the real AO devices in a wide range of optical wavelengths with high accuracy. This method makes it possible to simplify substantially the process of AO devices temperature calibrations.

Ultrasound attenuation was studied in a given AO cell in addition to the examination of temperature effect on the AO interaction characteristics. Attenuation exists due to the absorption of the acoustic wave power by the paratellurite crystal from which the AO cell is fabricated. Absorption is the main mechanism leading to the appearance of an inhomogeneous temperature distribution inside the AO cell when AO devices operate.

Examining the attenuation of ultrasonic waves, the following was discovered: the absorption of the power of acoustic waves by paratellurite is a very complicated process. It is necessary to investigate the acoustic anisotropy of tellurium dioxide for its description. It is shown that under the influence of absorption the shape of the AOTF transmission function changes. The presence of absorption leads to a decrease in the AO interaction efficiency, an increase of the AO filter passband, the smoothing of the transmission function side lobes was also observed.

Acknowledgements

This research has been supported by Russian Scientific Fund, Project 14-22-00042.

Appendix A. Supplementary material

Supplementary data associated with this article can be found, in the online version, at https://doi.org/10.1016/j.ultras.2018.07.016.

References

[1] J. Xu, R. Stroud, Acousto-Optic Devices, Wiley, New York, 1992.
[2] O.I. Korablev, et al., SPICAM IR acousto-optic spectrometer experiment on Mars Express, J. Geophys. Res. E 111 (2006) E09S03.
[3] V. Leroi, J.-P. Bibring, M. Berthe, MicrOmega/IR: design and status of a nearinfrared spectral microscope for in situ analysis of Mars samples, Planet. Space Sci. 57 (2009) 1068–1075.
[4] C. Pilorget, J.-P. Bibring, NIR reflectance hyperspectral microscopy for planetary science: application to the MicrOmega instrument, Planet. Space Sci. 76 (2013) 42–52.
[5] J.-L. Bertaux, et al., SPICAV/SOIR on Venus express: three spectrometers to study the global structure and composition of the Venus atmosphere, Planet. Space Sci. 55 (2007) 1653–1672.
[6] E. Dekemper, et al., Tunable acousto-optic spectral imager for atmospheric composition measurements in the visible spectral domain, Appl. Opt. 51 (2012) 6259–6267.
[7] O. Korablev, et al., Development of a mast or robotic arm-mounted infrared AOTF spectrometer for surface Moon and Mars probes, Proc. SPIE 9608 (2015) 960807.
[8] O.I. Korablev, et al., Infrared spectrometer for ExoMars:a mast-mounted instrument for the rover, Astrobiology 17 (2017) 542–564.
[9] D.A. Belyaev, et al., Compact acousto-optic imaging spectro-polarimeter for mineralogical investigations in near infrared, Opt. Exp. 25 (2017) 25980–25991.
[10] S.N. Mantsevich, O.I. Korablev, Yu.I. Kalinnikov, A.Yu. Ivanov, A.V. Kiselev, Wide-aperture TeO_2 AOTF at low temperatures: operation and survival, Ultrasonics 59 (2015) 50–58.
[11] V.Ya. Molchanov, V.M. Lyuty, V.F. Esipov, et al., An acousto-optical imaging spectrophotometer for astrophysical observations, Astron. Lett. 28 (2002) 713–720.
[12] S.N. Mantsevich, T.V. Yukhnevich, V.B. Voloshinov, Examination of the temperature influence on the acousto-optic filters performance, Opt. Spectr. 122 (2017) 675–681.
[13] J. Runhua, et al., Spatial and temporal thermal analysis of acousto-optic deflectors using finite element analysis model, Ultrasonics 52 (2012) 643–649.
[14] P. Maak, et al., Thermal behavior of acousto-optic devices: effects of ultrasound absorption and transducer losses, Ultrasonics 51 (2011) 441–451.
[15] Y. Ohmachi, N. Uchida, N. Niizeki, Acoustic wave propagation in TeO2 single crystal, J. Acoust. Soc. Am. 51 (1972) 164–168.
[16] V.I. Balakshy, S.N. Mantsevich, Propagation of acoustic beams in a paratellurite crystal, Acoust. Phys. 58 (2012) 549–557.
[17] H. Schweppe, Elastic and piezoelectric properties of paratellurite (TeO2), Ultrasonics 8 (1970) 84–87.
[18] Y. Ohmachi, N. Uchida, Temperature dependence of elastic, dielectric, and piezoelectric constants in TeO2 single crystals, J. Appl. Phys. 41 (1970) 2307–2311.
[19] I.M. Silvestrova, et al., Temperature dependence of elastic properties of paratellurite, Phys. Stat. Sol. 101 (1987) 437–444.
[20] H. Ledbetter, et al., Low-temperature elastic and piezoelectric constants of paratellurite, J. Appl. Phys. 96 (2004) 6201–6206.
[21] V. Balakshy, et al., Compensation of thermal effects in acousto-optic deflector, Proc. SPIE 2713 (1996) 164–171.
[22] S.N. Mantsevich, O.I. Korablev, Yu.I. Kalinnikov, A.Yu. Ivanov, A.V. Kiselev, Examination of temperature influence on wide-angle paratellurite crystal acousto-optic filters operation, Acta Phys. Pol. A 127 (2015) 43–45.
[23] V.I. Balakshy, V.N. Parygin, I.E. Chirkov, Physical Fundamentals of Acoustooptics, Radio i Svyaz', Moscow, 1985 (in Russian).
[24] G. Georgiev, David A. Glenar, John J. Hillman, Spectral characterization of acousto-

optic filters used in imaging spectroscopy, Appl. Opt. 41 (2002) 209–217.
[25] A. Yariv, P. Yeh, Optical Waves in Crystals, Wiley, N.Y, 1984.
[26] I.C. Chang, Noncollinear acousto-optic filter with large angular aperture, Appl. Phys. Lett. 25 (1974) 370.
[27] V.B. Voloshinov, Anisotropic light diffraction on ultrasound in a tellurium dioxide single crystal, Ultrasonics 31 (1993) 333–338.
[28] E. Dekemper, J. Vanhamel, B. Van Opstal, D. Fussen, V.B. Voloshinov, Influence of driving power on the performance of UV KDP-based acousto-optical tunable filters, J. Opt. 17 (2015) 075404.
[29] V.B. Voloshinov, E.A. Lemyaskina, Acousto-optic measurements of ultrasound attenuation in tellurium dioxide crystal, Acta Phys. Slovaca 46 (1996) 733–738.
[30] S. Antonov, E. Kuznetsova, V. Mirgorodsky, V. Proklov, Acousto-optic examination of slow acoustic wave propagation in TeO_2, Sov. J. Acoust. 4 (1982) 433–437.